



Power Electronic Systems  
Laboratory

© 2016 IEEE

Proceedings of the 31st Applied Power Electronics Conference and Exposition (APEC 2016), Long Beach, CA, USA, March 20-24, 2016

## **Comparison of Lateral- and Cylindrical-Stator Electrical Machines for High-Speed Direct-Drive Applications in Confined Spaces**

A. Tüysüz  
J. W. Kolar

This material is published in order to provide access to research results of the Power Electronic Systems Laboratory / D-ITET / ETH Zurich. Internal or personal use of this material is permitted. However, permission to reprint/republish this material for advertising or promotional purposes or for creating new collective works for resale or redistribution must be obtained from the copyright holder. By choosing to view this document, you agree to all provisions of the copyright laws protecting it.



Eidgenössische Technische Hochschule Zürich  
Swiss Federal Institute of Technology Zurich

# Comparison of Lateral- and Cylindrical-Stator Electrical Machines for High-Speed Direct-Drive Applications in Confined Spaces

Arda Tüysüz and Johann W. Kolar  
Power Electronic Systems Laboratory, ETH Zurich  
Email: tuysuz@lem.ee.ethz.ch

**Abstract**—Lateral-Stator Machine (LSM) topology is presented in earlier works as an unconventional machine that is advantageous for high-speed, direct-drive applications in confined spaces. Owing to its peculiar geometry, LSM makes use of the additional space in a tool head that cannot be utilized by standard Cylindrical-Stator Machines (CSMs). However, a fair and quantitative comparison of LSM and CSM topologies has not been carried out so far. This paper presents a comparative evaluation of the LSM against slotless and slotted permanent-magnet CSMs, not only in terms of torque density but also concerning torque ripple and self-sensing control capability.

## I. INTRODUCTION

The Lateral-Stator Machine (LSM) is introduced in [1], for directly driven high-speed machining applications where the space at the tool head is limited, and where the electrical machine can grow only in one lateral direction. A typical example are dental drills, where ergonomic constraints limit the size of the handpiece.

The LSM topology can be seen in Fig. 1(a). As shown in Fig. 1(b), in a state-of-the-art dental handpiece, a standard, Cylindrical-Stator Machine (CSM) is placed in the handpiece body, where the available space is larger. Several stages of mechanical transmission are used to connect the machine to the drill and to increase the speed from around 40 000 r/min up to around 200 000 r/min. A high-speed CSM placed directly in the head of the handpiece would enable a direct drive and omit the need for mechanical transmissions; however, the space at the tool head is small and a CSM fitting there could potentially not deliver the torque required by the application. In contrast, an LSM can be accommodated in the tool head and drive the drill directly as shown in Fig. 1(c).

Due to the peculiar shape of its stator extending laterally only on one side, the LSM makes use of the space at the tool neck, which would not be used for magnetic parts in case of the conventional CSMs. Therefore, the same tool is able to deliver a higher power output when directly driven by an LSM, compared to a direct drive realized with a CSM. However, so far no quantitative comparison is made between these two types of electrical machines. Thus, this paper deals with the comparative evaluation of the LSM versus two types of permanent-magnet (PM) CSM topologies, namely the slotless and slotted machine types.

Slotless PM machines have a large magnetic air gap and are therefore characterized by weak armature reaction and consequently lower rotor losses caused by the harmonic content

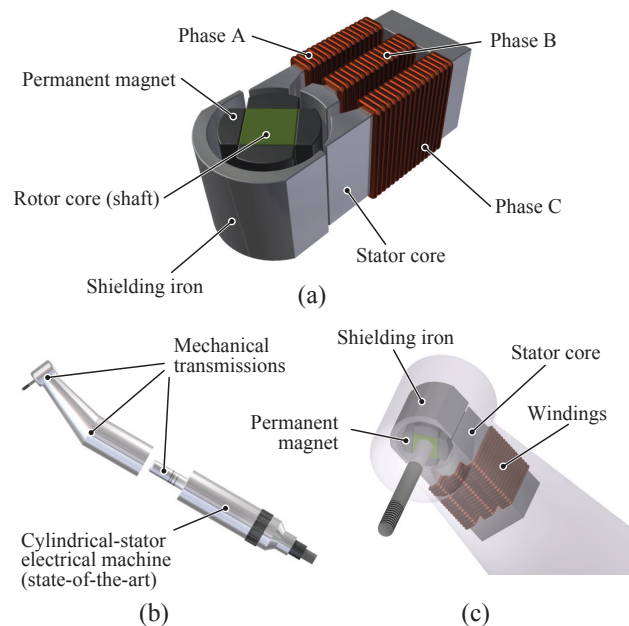


Fig. 1. (a) Conceptual drawing of the Lateral-Stator Machine (LSM). (b) State-of-the-art electric dental handpiece. The rated speed of the electric machine is around 40 000 r/min. Mechanical step-up transmission stages are used to connect the machine to the drill, whose rated speed is 200 000 r/min. (c) An LSM fits in the tool head and can deliver the required torque without using gearboxes. As the stator core is extended on one lateral side, space is gained for the windings outside the tool head [2].

of the armature current [3]. Moreover, this machine type does not suffer from no-load rotor eddy-current losses due to the constant air gap permeance. Thus, it is well suited for high-speed drives. For example, a 500 000 r/min electrical machine is designed in [4], and another one running at 1 000 000 r/min in [5], both with a slotless stator and a one-piece, diametrically magnetized PM rotor.

Even though they are better suited for high-speed applications, the torque density of slotless machines is lower compared to their slotted counterparts [6]. Slotted machines with concentrated (non-overlapping) windings offer higher torque densities due to their shorter end windings compared to machines with overlapping windings [7]. Therefore, they are more commonly used in low-speed, high torque density

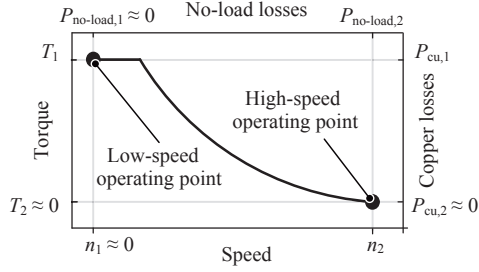


Fig. 2. Typical torque-speed plane of machining applications such as dental drills.

applications such as robotics and power steering [8].

Therefore, this paper compares the LSM topology to the slotless machine type with one pole pair and to the slotted machine type with higher number of poles and concentrated windings. Although the latter is not a very suitable machine topology for high-speed applications due to the higher core losses as a result of the higher electrical frequency and higher no-load rotor losses caused by the non-constant air gap permeability, it is still interesting to compare its torque capability with that of the LSM for applications in confined spaces. Moreover, torque ripple and self-sensing capability of the machines are also discussed.

## II. ELECTROMAGNETIC MODELING OF THE MACHINES

### A. Target Specifications and Optimization

Various high-speed micro-machining applications ranging from dental drills to high-precision manufacturing tools require electric drives that can deliver high torque at low speeds, while generating low losses at high speeds under low loads. This results in the torque-speed plane illustrated in Fig. 2. Copper (Joule) losses are the only loss component considered in the low-speed operating point whereas they are neglected at the high-speed operating point, where only the no-load losses are considered.

In the LSM optimization presented in [1], the goal is defined as finding the machine geometry that generates the highest torque  $T_1$  for a given  $P_{cu,1}$ , while generating less no-load losses than a defined  $P_{no-load,2}$  at the speed  $n_2$ . Based on thermal capacitances and assumptions on the drive cycle,  $P_{cu,1}$  is set to 6 W and  $n_2$  is set to 200 000 r/min. In this work, the same specifications are assumed for a direct comparison of the machine types. However, as the main focus is on the torque capabilities of different machine types, the rotor eddy-current losses are neglected.

### B. Lateral-Stator Machine

Partial saturation of the stator and the leakage flux between the stator legs play a very important role in determining the performance of the LSM. In order to capture these effects accurately, Two-Dimensional (2-D) Finite-Element Method (FEM) is used for modeling the LSM. The machine geometry is parametrized as shown in Fig. 3(a). Table I shows the discretization of the design space. For each machine in the design space, the winding resistance is calculated assuming

TABLE I. DISCRETIZATION OF THE GEOMETRIC DESIGN SPACE

LSM	$w_s$	Shaft width	3.5, 4 mm
	$r_r$	Rotor radius	3.4 mm
	$w_n$	Tool neck width	8 mm
	$w_h$	Tool head width	8.8 mm
	$l_s$	Stator length	10 to 25 mm, 4 steps
	$\tau$	Shoe span	40, 45 deg
Slotless	$w_1$	Leg width	0.8 to 1.4 mm, 4 steps
	$r_s$	Stator outer radius	4 mm
	$r_r$	Rotor radius	0.4 to 2.8 mm, 7 steps <sup>1</sup>
	$t_w$	Winding thickness	0.4 to 2.8 mm, 7 steps <sup>1</sup>
	$r_s$	Stator outer radius	4 mm
	$r_b$	Stator bore radius	1 to 3.5 mm, 15 steps <sup>2</sup>
Slotted	$t_m$	Magnet thickness	0.5 to 3.5 mm, 15 steps <sup>2</sup>
	$\tau Q/2\pi$	Tooth coverage	0.6 to 0.85, 5 steps
	$\alpha p/\pi$	Magnet coverage	0.6 to 1, 5 steps
	$p/Q$	Pole-pair/Slot number	2/6, 3/9, 4/12, 5/15, 6/18
All	$l_a$	Active length <sup>3</sup>	7.4 mm

<sup>1</sup> Excluding designs where the resulting stator core thickness is below 0.2 mm.

<sup>2</sup> Excluding designs where  $r_b - t_m < 0.6$  mm.

<sup>3</sup> Axial length of the stator core and the PMs perpendicular to the page plane.

a slot fill factor of 0.3; and a sinusoidal current amplitude is calculated accordingly, such that the total copper losses are  $P_{cu,1} = 6$  W. The mean value of the torque is calculated over an electrical period. A second FEM model is run at 200 000 r/min under no load to calculate the stator core losses. Amorphous iron with 23  $\mu\text{m}$  lamination thickness is considered as core material and NdFeB magnets with a remanent flux density of 1.1 T are assumed in the rotor.

A 0.2 mm thick hollow-cylinder-shaped sleeve is assumed on the rotor to hold the permanent magnets in their place under the strong centrifugal stresses occurring at high rotational speeds. The mechanical air gap is constant at 0.2 mm. A 0.2 mm thick plastic hollow cylindrical wall that is coaxial to the rotor separates the mechanical air gap from the lateral stator and the shielding iron. As the sleeve and the plastic wall are made of non-magnetic materials, they are not included in the FEM models. The resulting magnetic air gap is 0.6 mm in the analyzed machines.

Air-friction losses are calculated according to [9]. Further details about the modeling approach can be found in [1].

### C. Slotless topology

Fig. 3(b) shows a cross-sectional view of the slotless machine. The stator core is a hollow cylinder with no slots. The air gap windings are usually made of Litz wire (with strand diameters as small as e.g. 50  $\mu\text{m}$ ) in order to limit the skin and proximity losses. The rotor consists of a one-piece, diametrically magnetized, cylindrical permanent magnet. As shown in Fig. 4, the torque is transferred to the load using a sleeve that also forms a shaft.

Analytical field models have been presented in literature for analyzing the performance of slotless PM machines [9]. Nevertheless, since only two independent parameters are sufficient to define a unique machine (cf. Table I), 2-D FEM is used in this work for modeling the slotless machine as well. The rotor radius  $r_r$  and the winding thickness  $t_w$  are both swept from 0.4 mm to 2.8 mm, excluding the designs where the resulting stator core thickness is below 0.2 mm. Core and magnet materials as well as the machine's active length and



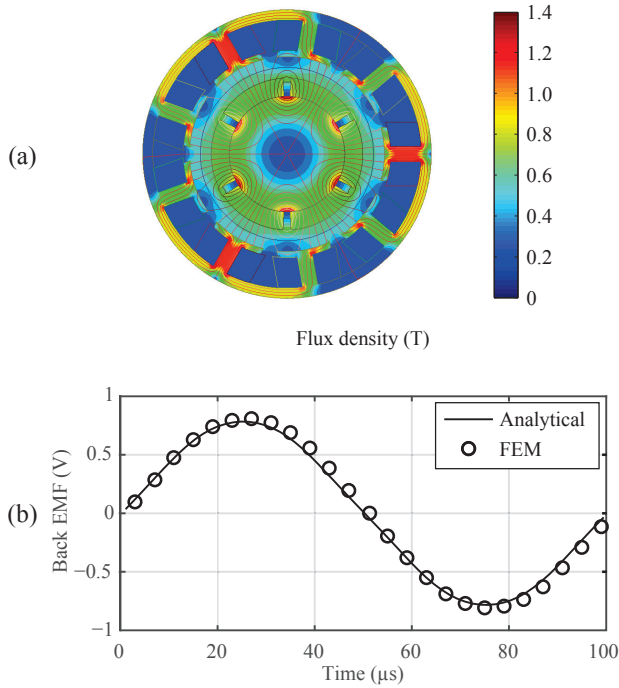


Fig. 5. (a) 2-D FEM simulation results showing the no-load flux distribution of a 3-pole, 9-slot machine with  $r_b = 2.7$  mm,  $t_m = 0.5$  mm,  $\frac{\alpha p}{\pi} = 0.9$ ,  $\frac{\tau Q}{2\pi} = 0.8$ ,  $w_1 = 0.42$  mm and  $h_s = 0.17$  mm. It can be seen that the maximum flux density in the stator is equal to  $B_{sat}$  (saturation flux density of the core material is 1.56 T, and the stacking factor is 84%; hence, the effective saturation flux density is  $B_{sat} = 1.56$  T  $\cdot$  0.84 = 1.3 T). (b) The back EMF of the same machine at 200 000 r/min. The windings of the machine are double-layer concentrated windings and the number of winding turns is one.

Before analyzing all the machines in the parameter range given in Table I, the analytical model described above is verified using 2-D FEM analysis for a single machine geometry. A very high constant relative permeability ( $\mu_r = 100\ 000$ ) is assumed in the stator core to approximate the infinite permeability assumed in the analytical approach. Fig. 5(a) shows the no-load flux distribution in this machine. It can be seen that the tooth width and the tooth tip height are calculated properly as the maximum flux density in the stator is equal to the saturation flux density of the core material (saturation flux density of the core material itself is 1.56 T, and the stacking factor is 84%; hence, the effective saturation flux density is  $B_{sat} = 1.56$  T  $\cdot$  0.84 = 1.3 T). Fig. 5(b) shows the back EMF of this machine for one winding turn and 200 000 r/min, as calculated by analytical and FEM models. These results verify the use of analytical models for the optimization of the slotted machine. Similar to the LSM and the slotless machine types, all slotted machines in the design space are evaluated by first estimating the winding resistance based on the machine geometry, and then calculating the torque for a sinusoidal machine current that generates the copper losses  $P_{cu,1} = 6$  W. Core and magnet materials as well as the machine's active length are the same as for the LSM and the slotless machine.

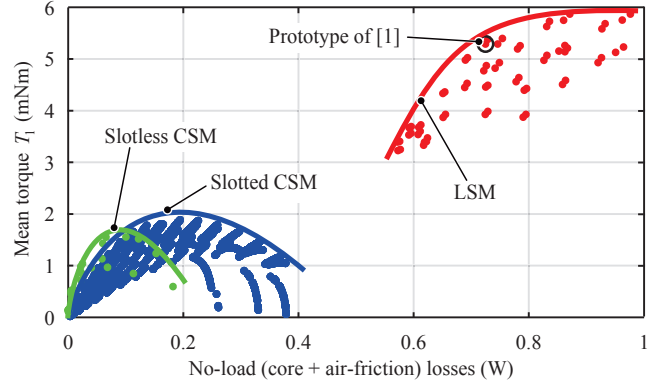


Fig. 6. Comparative evaluation of the performances of two CSMs and the LSM. y-axis shows the mean torque of the machines when producing 6 W of copper losses. x-axis shows the no-load (stator core and air friction) losses at 200 000 r/min.

TABLE II. SLOTLESS AND SLOTTED CSMs THAT PRODUCE THE HIGHEST TORQUE

Slotless	$r_r$	Rotor radius	2 mm
	$t_w$	Winding thickness	0.8 mm
	$\Psi$	Flux linkage per turn	13.9 $\mu$ Wb
	$T_1$	Torque	1.55 mNm
	$P_c$	Stator core losses	54 mW
	$P_{air}$	Air-friction losses	65 mW
Slotted	$r_b$	Stator bore radius	2.6 mm
	$t_m$	Magnet thickness	0.71 mm
	$\tau Q/2\pi$	Tooth coverage	0.6 mm
	$\alpha p/\pi$	Magnet coverage	1 mm
	$p/Q$	Pole-pair/Slot number	3/9
	$w_1$	Tooth width	0.42 mm
	$h_s$	Shoe height	0.16 mm
$\Psi$	Flux linkage per turn	12.1 mWb	
$T_1$	Torque	1.88 mNm	
$P_c$	Stator core losses	128 mW	
$P_{air}$	Air-friction losses	65 mW	

### III. COMPARISON OF (LOCAL) TORQUE DENSITIES

Fig. 6 shows the mean torque and no-load losses of all the analyzed machines. Each dot in this plot represents a unique machine in the design space. It can be seen clearly that for the same radial space in the tool head, the same active length and the same copper losses, the LSM topology enables significantly higher torque output than both the slotted and the slotless CSMs. Table II describes the slotted and slotless CSMs that produce the highest torque in the analyzed design space.

Certain assumptions made during the modeling process have to be considered for a correct interpretation of Fig. 6. For instance, the same active length is assumed for all the machines. However, due to the straight and overlapping windings with 180° pitch, the slotless machine requires considerably larger space for the end windings compared to the LSM. Consequently, a shorter active length needs to be considered for the slotless machine if it must fit in the same space as the LSM.

As only double-layer concentrated windings are considered in the slotted machine, the space needed for the end windings is less than what is needed for the end windings of the slotless machine. This is illustrated in Fig. 7. However, the end windings still need to be placed in the head of the tool,

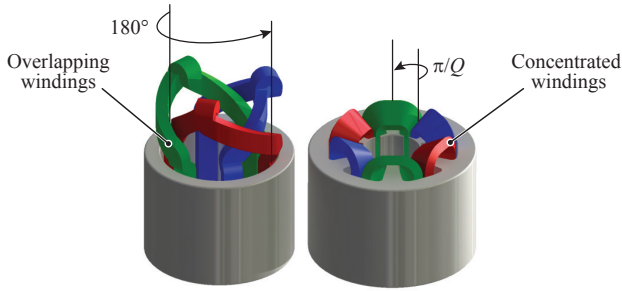


Fig. 7. End windings of the slotless machine with straight and overlapping windings with  $180^\circ$  pitch (left), and slotted machine with double-layer non-overlapping (concentrated) windings. The end winding overhead is smaller for the slotted machine with concentrated windings.

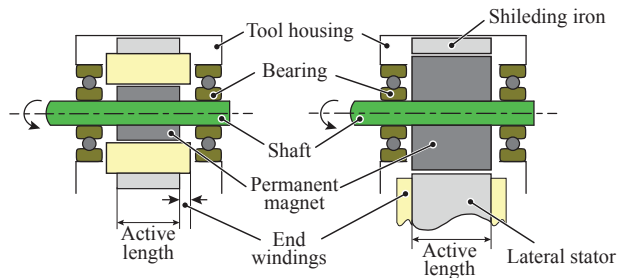


Fig. 8. Positioning of a CSM with end windings (left) and an LSM (right) in the same tool. The end windings of the CSM and the bearings need to fit in the same space, limiting the maximum active (axial) length of the machine. As the windings are taken out of the tool head, the LSM can have not only a radially larger but also an axially longer rotor compared to the CSM.

which is not the case for the LSM, as shown in Fig. 8. Hence, even if the axial length of the end winding is similar for a slotted CSM and an LSM, the LSM can still have a larger active length (axially longer rotor) as its end windings are not in the tool head.

It is clear that incorporating the considerations related to the end windings in the models will change the results shown in Fig. 6 only in favor of the LSM, which can produce significantly higher torque than both types of CSMs even when the same active length is assumed. Therefore, the effect of end windings are not studied any further in this paper.

A direct comparison of the slotted and slotless CSM types, on the other hand, requires a careful consideration of the winding structures. Rotor dynamics may impose a limit on the maximum rotor length in high-speed drives, which makes the end winding overhead a very undesirable feature as it leads to a longer rotor without actually increasing the machine's active length. In practice, ultra-high-speed machines are usually realized using rhombic or skewed air gap windings to shorten or fully avoid the end windings [11]. This, however, reduces the winding factor and the torque-per-current rating of the machine. Nevertheless, this is not studied any further here as the main focus of this paper is not the detailed comparison of the slotted and slotless CSM types to each other.

Moreover, the same copper losses ( $P_{cu,1} = 6 \text{ W}$ ) are as-

sumed in this paper for all the three machine types, for a direct comparison of the machine structures without considerations about cooling. However, a CSM that fits in the tool head has smaller surface for cooling compared to an LSM, hence, its electrical loading may not be as high as that of the LSM. For this reason, the comparison of torque capability is expected to change even more in favor of the LSM following a detailed thermal analysis of both machine types. If Fig. 6 is interpreted considering the remarks about the end windings and the thermal aspects, it can be concluded that the LSM produces *at least* three times the torque that a CSM can offer for a given machining tool.

It has to be noted that so far only applications with a limited space around the rotor have been considered where the stator of the LSM can grow in one lateral direction. Clearly, this gives an advantage to the LSM when comparing the maximum torque that can be generated, as the LSM can utilize more active material (permanent magnets, copper and iron). To be fair, it has to be mentioned that it is the *local* torque density that increases when using an LSM. The *overall* torque density of the LSM prototype of [1] is  $3.9 \text{ mNm/cm}^3$ , whereas the *overall* torque density of the slotless and slotted CSMs of Table II is  $4.2 \text{ mNm/cm}^3$  and  $5.1 \text{ mNm/cm}^3$ , respectively. Furthermore, it has to be also noted that the volumetric scalability of the LSM is not similar to that of the CSM due to the stray field between the stator legs in an LSM. That is, increasing the stator length  $l_s$  of an LSM results in higher total slot current for the same copper losses and increases the torque output until an optimum  $l_s$  value; but beyond that, effect of the stray field becomes visible and the torque output of the machine does not increase further.

#### IV. LSM VERSUS CSM: FURTHER ASPECTS

##### A. Torque ripple

Torque ripple is an undesired effect in applications like machining spindles and dental drills especially at low speeds as it may lead to acoustic noise and vibration. Slotless machines analyzed in this work have a perfectly smooth magnetic circuit and exhibit no cogging torque. The flux linkage is also very sinusoidal, leading to a ripple-free torque when the machine is driven by sinusoidal currents. On the other hand, these machines are also characterized by low phase inductances due to the large magnetic air gap, which means that the drive inverter needs to operate with a high switching frequency and/or a filter needs to be incorporated between the machine and the inverter, in order to drive the machine with sinusoidal currents with low harmonic content. In order to avoid high switching losses and the additional space requirement of filters, Pulse-Amplitude Modulation (PAM) has also been widely applied in inverters driving high-speed slotless machines [13]. However, the block-shaped current waveform resulting from PAM operation leads to torque ripple in machines with sinusoidal back EMF. On the other hand, recent developments in wide-bandgap devices such as Gallium-Nitride (GaN) power switches enable a feasible operation of drive inverters with high switching frequencies, facilitating a clean drive current supply even for very low-inductance machines [14]. For this reason, a purely sinusoidal drive current is assumed in this work for all the analyzed machines.

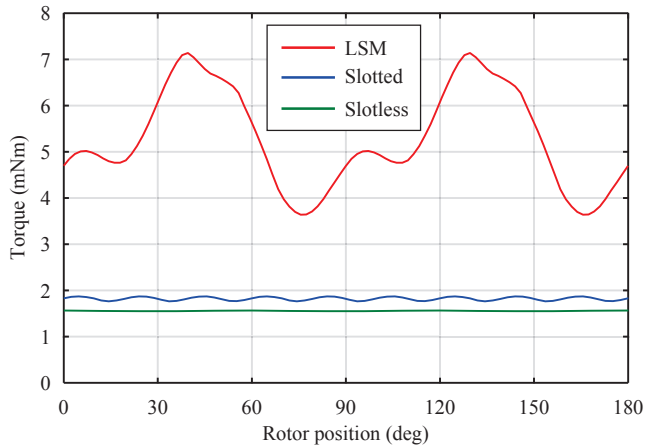


Fig. 9. 2-D FEM simulation results showing the torque of the LSM prototype [1] and the CSMs designs given in Table II. Copper losses are  $P_{cu,1} = 6$  W for all the machines.

Slotted machines suffer from cogging torque due to the attraction between the magnets and the stator tooth tips. The distorted air gap flux distribution also contributes to the torque ripple observed in these machines. On the other hand, the pole-slot combination offers a degree of freedom that can be exploited to minimize the torque ripple [15]. The analytical modeling approach used for the slotted machines in this work only calculates the mean torque. A 2-D FEM model with constant permeability, such as the one used to verify the analytic approach in Section II-D, cannot estimate the torque ripple either, as the influence of the magnetic saturation cannot be captured. Therefore, in this section, a 2-D FEM model that incorporates the nonlinear permeability of the stator core is used –identical to the models used for the lateral-stator and slotless machines– for assessing the torque ripple of the slotted machine.

Fig. 9 shows the torque generated by the LSM described in [1], and the CSMs described in Table II. All three machines are driven by three-phase sinusoidal currents resulting in  $P_{cu,1} = 6$  W copper losses. As expected, the slotless machine generates a virtually ripple-free torque, whereas the peak-to-peak ripple is as large as two thirds of the mean torque for the LSM. The slotted machine exhibits a torque ripple whose peak-to-peak value is around 5% of its mean torque. The mean torque of this machine is predicted as 1.88 mNm by the analytic models and as 1.82 mNm by the 2-D FEM simulation incorporating the nonlinear magnetic permeability. Hence, the use of the analytic models is verified once more.

### B. Unbalanced magnetic pull

In state-of-the-art permanent-magnet electric machines with cylindrical stators, rotor eccentricity and/or uneven magnetization of permanent magnets may lead to an unbalanced magnetic pull on the rotor [16], [17]. The unbalanced magnetic pull may excite vibrations and shorten the lifetime of the bearings. On the other hand, the asymmetric structure of the LSM results in large magnetic forces acting on the shielding iron, the rotor and the lateral stator, even in the absence of any rotor eccentricity or uneven permanent-magnet magnetization.

Forces up to 7 N pull both the lateral-stator and the shielding iron towards the rotor. As shown in [18], a 3-D printed, 0.2 mm thick plastic wall can withstand these forces. However, long lifetime tests are required to characterize the effect of these forces on the lifetime of the bearings.

### C. Position sensing

Rotor position of a PM synchronous machine is needed for a closed-loop operation. A simple way of obtaining the rotor position information is by using dedicated position sensors such as encoders, resolvers or Hall sensors. However, for drive applications in confined spaces as studied in this paper, the space required by an off-the-shelf position sensor may easily be significant compared to the size of the machine, meaning that the machine needs to be built considerably smaller in order to accommodate the position sensor. Consequently, the use of a dedicated position sensor may result in a sizable decrease in the torque that can be generated. For that reason, the possibility of obtaining the rotor position without the use of dedicated position sensors (self-sensing operation) is discussed in the following, for the machines under consideration.

The back EMF of an electrical machine depends on the rotor position, and it can be either measured or estimated using an observer for estimating the rotor position. However, this method is not considered in this paper since it is not applicable for the whole speed range, considering that the back EMF gets more difficult to measure at low speeds and vanishes at standstill. The variation of the machine impedance with the rotor position, on the other hand, can be exploited for position estimation also at lower speeds.

The symmetrical construction of the slotless machine type leads to a virtually non-existent dependency of the machine impedance on the rotor position. Nevertheless, the anisotropic properties of rare-earth magnets introduce a small saliency. Special arrangements of high-frequency signal injection and measurement circuitry have been presented in [19] and [20] for detecting saliencies as small as a few percent. When a metallic sleeve is used on the rotor, alteration of the sleeve geometry may introduce an additional, designer-controlled spatial saliency in the rotor surface resistance [21], which can be detected by a high-frequency signal superimposed on the machine current. However, these methods come with various drawbacks, such as the increased system complexity, the need of using a filter between the machine and the inverter, or the need for having an accessible star-point connection in the machine, or modifying the geometry of the rotor sleeve - a part whose design is subject to very tight tolerances and mechanical constraints. Hence, the reliable and cost-effective self-sensing operation of slotless CSMs in the full speed range remains to be a challenge.

Saliency-tracking-based self-sensing operation of slotted CSMs has been studied extensively in the recent years [22]. Even though surface-mounted PM machines studied in this paper feature a smaller spatial variation of impedance compared to e.g. interior PM machines, observers can be used for increasing the signal-to-noise ratio of the tracked saliency signal, thereby enabling a closed-loop self-sensing operation [23].

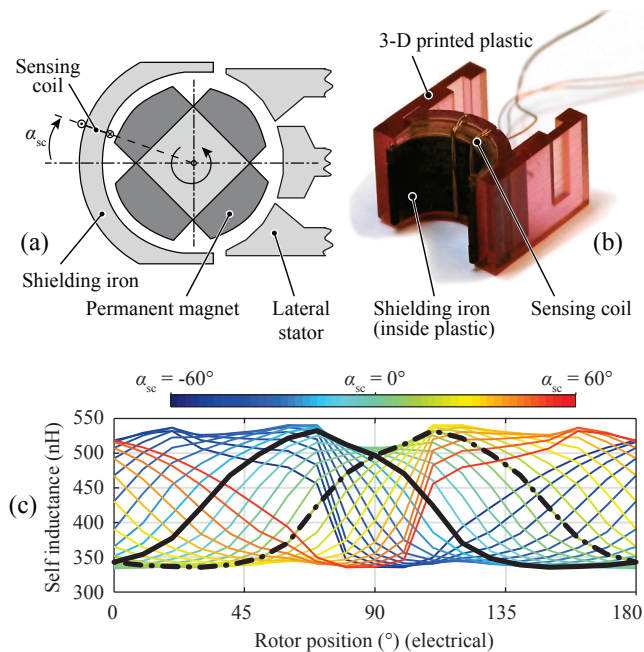


Fig. 10. (a) Illustration of an LSM with a sensing coil wound around the shielding iron. (b) Photograph of a shielding iron with two sensing coils wound on it. The iron is placed inside a 3-D printed plastic case that facilitates the positioning of the shielding iron and the winding of the sensing coil. (c) 2-D FEM analysis results showing the self inductances of the sensing coils placed at positions from  $-60^\circ$  to  $60^\circ$ . Solid and dashed black lines show  $\alpha_{sc} = -15^\circ$  and  $\alpha_{sc} = 15^\circ$  [2].

In principle, any self-sensing method that can be used for a slotted CSM can also be applied to an LSM, which is by no means a low-saliency machine. On the other hand, an LSM optimized for the highest torque and lowest losses is not necessarily suitable for self-sensing position estimation. For example, all the self and mutual inductances of the LSM optimized in [1], go flat at the same rotor position, making an impedance-tracking-based self-sensing method go blind at these rotor positions [2]. Moreover, the stator core of this machine operates in partial saturation already at no load; hence, the dependency of the impedance on the rotor position is heavily influenced by the load of the machine.

A new position sensing method is presented in [2] for LSMs, where the rotor-position-dependent impedance of the sensing coils wound on the shielding iron is measured by a high-frequency current injection. Even though this is not a self-sensing method, it does not need a large additional space since the sensor is integrated into the machine. Moreover, the magnetic circuit of the sensing coil is largely decoupled from the stator-field, making the position estimation method much less sensitive to machine's load. Fig. 10(a) and Fig. 10(b) show how the sensing coils are wound on the shielding iron. The rotor-position-dependent variation of the self inductance of a sensing coil wound on the shielding iron at different positions is depicted in Fig. 10(c).

## V. HARDWARE AND MEASUREMENTS

Fig. 11 shows a photograph of the rotor of an LSM. Permanent magnets are retained using a titanium sleeve. The

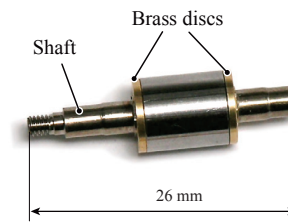


Fig. 11. Rotor of the LSM prototype described in [1]. A long shaft with a thread on one end is used for coupling the LSM to another machine during measurements.

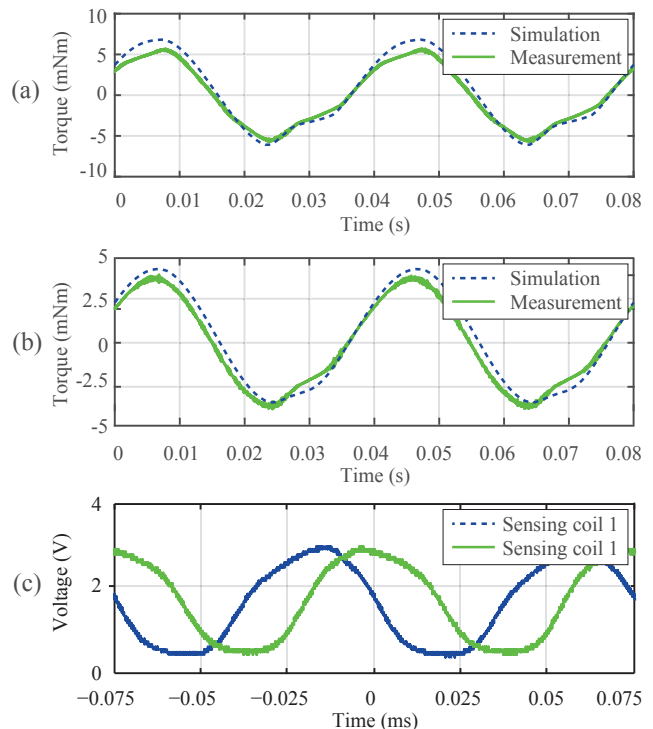


Fig. 12. Simulated and measured torques of an LSM with 33 winding turns when the rotor is fixed for a peak phase current of (a) 5 A, and (b) 3 A. (c) Demodulated and filtered voltage response of the sensing coils measured at 200 000 r/min. The injection frequency is 1 MHz [2].

two brass discs on both axial ends of the sleeve are used for balancing the rotor.

A bearingless standstill torque measurement setup, whose details can be found in [18], is used for verifying the torque capability of the LSM while avoiding bearing friction in the measurements. As seen in Fig. 12(a,b), the FEM models predict the measured torque accurately, which verifies the modeling approach adopted for the optimization of the LSM. Fig. 12(c) shows the filtered and demodulated rotor-position-dependent voltage responses of two sensing coils wound on the shielding iron at  $\alpha_{sc} = -15^\circ$  and  $\alpha_{sc} = 15^\circ$ , for a rotational speed of 200 000 r/min. A digital signal processor sampling these voltages can estimate the rotor position using a simple look-up table [2].

## VI. CONCLUSIONS AND OUTLOOK

The Lateral-Stator Machine (LSM) has been proposed in earlier works for high-speed, direct drive applications in confined spaces. However, a quantitative comparison of this machine type to standard, Cylindrical-Stator Machine (CSM) topology has not been carried out so far. This paper compares the LSM to two commonly used CSM types, namely the slotless permanent-magnet machine with one pole pair, and the slotted surface-mount permanent-magnet machine with higher number of pole pairs and concentrated windings. Both analytical and FEM field models are used to compare the torque capabilities of the two CSM types versus the LSM. Due to the peculiar arrangement of its stator, the LSM can make use of the space that cannot be utilized by standard machines, and therefore it can generate at least three times the torque standard machines can offer for the same machining tool. On the other hand, due to the inherent features of the LSM such as the stray field between the legs and the shielding iron that does not contribute to torque generation, the overall torque density of the LSM ( $3.9 \text{ mNm/cm}^3$ ) is lower than that of both the slotless ( $4.2 \text{ mNm/cm}^3$ ) and the slotted ( $5.1 \text{ mNm/cm}^3$ ) CSMs. Moreover, the LSM exhibits a large magnetic pull, whose effect on the bearing lifetime needs to be studied.

By the integration of sensing coils in the machine design, the LSM can be operated closed-loop in the whole speed range without the need for dedicated position sensors.

## ACKNOWLEDGMENT

The authors would like to express their sincere appreciation to Celeroton AG for the continuous support they provided during the design, construction and testing of the lateral-stator machine. The authors also acknowledge the support of CADFEM (Suisse) AG concerning the ANSYS software.

## REFERENCES

- [1] A. Tüysüz, C. Zwyssig, J. W. Kolar, "A novel motor topology for high-speed micro-machining applications," *IEEE Trans. Ind. Electr.*, vol. 61, no. 6, pp. 2960-2968, Jun. 2014.
- [2] A. Tüysüz, J. W. Kolar, "New position sensing concept for miniature lateral-stator machines," *IEEE Trans. Ind. Electr.*, accepted for publication in Nov. 2015.
- [3] N. Bianchi, S. Bolognani, F. Luise, "Potentials and limits of high-speed PM motors," *IEEE Trans. Ind. Appl.*, vol. 40, no. 6, pp. 1570-1578, Nov./Dec. 2004.
- [4] D. Krähenbühl, C. Zwyssig, H. Weser, J. W. Kolar, "A miniature 500 000-r/min electrically driven turbocompressor," *IEEE Trans. Ind. Appl.*, vol. 46, no. 6, pp. 2459-2466, Nov./Dec. 2010.
- [5] C. Zwyssig, S. Round, J. W. Kolar, "Megaspeed drive systems: Pushing beyond 1 million r/min," *IEEE/ASME Trans. Mech.*, vol. 14, no. 5, pp. 564-574, Oct. 2009.
- [6] J. W. Kolar, T. Friedli, F. Krismer, A. Looser, M. Schweizer, R. Friedemann, P. Steimer, J. Bevirt, "Conceptualization and multi-objective optimization of the electric system of an airborne wind turbine," *IEEE Jour. Emerg. Sel. Top. Pow. Electr.*, vol. 1, no. 2, pp. 72-103, Jun. 2013.
- [7] J. Cros, P. Viarouge, "Synthesis of high performance PM motors with concentrated windings," *IEEE Trans. Ene. Conv.*, vol. 17, no. 2, pp. 248-253, Jun. 2002.
- [8] K. Wang, Z. Q. Zhu, G. Ombach, M. Koch, S. Zhang, J. Xu, "Electromagnetic performance of an 18-slot/10-pole fractional-slot surface-mounted permanent-magnet machine," *IEEE Trans. Ind. Appl.*, vol. 50, no. 6, pp. 3685-3696, Nov./Dec. 2014.
- [9] J. Luomi, C. Zwyssig, A. Looser, J.W. Kolar, "Efficiency optimization of a 100 W 500 000 r/min permanent-magnet machine including air-friction losses," *IEEE Trans. Ind. Appl.*, vol. 45, no. 4, pp. 1368-1377, Jul./Aug. 2009.
- [10] C. Zwyssig, D. Krähenbühl, H. Weser, J. W. Kolar, "A miniature turbocompressor system," *Proc. of Smart Ene. Strat.*, (SES), Zurich, Switzerland, Sep. 2008.
- [11] A. Looser, T. Baumgartner, J. W. Kolar, C. Zwyssig, "Analysis and measurement of three-dimensional torque and forces for slotless permanent-magnet motors," *IEEE Trans. Ind. Appl.*, vol. 48, no. 4, pp. 1258-1266, Jul. 2012.
- [12] Z. Zhu, D. Howe, E. Bolte, and B. Ackermann, "Instantaneous magnetic field distribution in brushless permanent magnet DC motors. I. Open-circuit field," *IEEE Trans. Ind. Appl.*, vol. 29, no. 1, pp. 124-135, Jul. 1993.
- [13] L. Schwager, A. Tüysüz, C. Zwyssig, J. W. Kolar, "Modeling and comparison of machine and converter losses for PWM and PAM in high-speed drives," *IEEE Trans. Ind. Appl.*, vol. 50, no. 2, pp. 995-1006, Mar./Apr. 2012.
- [14] A. Tüysüz, R. Bosshard, J. W. Kolar, "Performance comparison of a GaN GIT and a Si IGBT for high-speed drive applications," *Proc. of Intl. Pow. Electr. Conf.*, (ECCE Asia, IPEC), Hiroshima, Japan, May 18-21, 2014.
- [15] J. A. Güemes, A. M. Iraolagoitia, J. I. Del Hoyo, P. Fernandez, "Torque analysis in permanent-magnet synchronous motors: A comparative study," *IEEE Trans. Ene. Conv.*, vol. 26, no. 1, pp. 55-63, Mar. 2011.
- [16] M. Michon, K. Atallah, G. Johnstone, "Effects of unbalanced magnetic pull in large permanent magnet machines," *Proc. of Ene. Conv. Cong. Expo.*, (ECCE), pp. 4815-4820, Pittsburgh, USA, Sep. 2014.
- [17] M. Novak, M. Kosek, "Unbalanced magnetic pull induced by the uneven rotor magnetization of permanent magnet synchronous motor," *Proc. of 11<sup>th</sup> Intl. ELEKTRO Conf.*, pp. 347-351, Rajecke Teplice, Slovakia, May 2014.
- [18] A. Tüysüz, D. Koller, A. Looser, J. W. Kolar, C. Zwyssig, "Design of a test bench for a lateral stator electrical machine," *Proc. of 37<sup>th</sup> IEEE Ann. Conf. Ind. Electr. Soc.*, (IECON), pp. 1801-1806, Melbourne, Australia, Nov. 2014.
- [19] A. Tüysüz, M. Schöni, J. W. Kolar, "Novel signal injection methods for high-speed self-sensing electrical drives," *Proc. of Ene. Conv. Cong. Expo.*, (ECCE), pp. 4815-4820, Raleigh, USA, Sep. 2012.
- [20] J. Persson, M. Markovic, Y. Perriard, "A new standstill position detection technique for nonsalient permanent-magnet synchronous motors using the magnetic anisotropy method," *IEEE Trans. on Magn.*, vol. 43, no. 2, pp. 554-560, Feb. 2007.
- [21] J.-P. Voillat, "Device for controlling an electric motor," *U.S. Patent*, 6 337 554 B1, Jan. 2002.
- [22] X. Wang, W. Xie, G. Dajaku, R. Kennel, D. Gerling, R. D. Lorenz, "Position self-sensing evaluation of novel CW-IPMSMs with an HF injection method," *IEEE Trans. Ind. Appl.*, vol. 50, no. 5, pp. 3325-3334, Sep./Oct. 2014.
- [23] S.-C. Yang, R. D. Lorenz, "Surface permanent-magnet machine self-sensing at zero and low speeds using improved observer for position, velocity, and disturbance torque estimation," *IEEE Trans. Ind. Appl.*, vol. 48, no. 1, pp. 151-160, Jan./Feb. 2012.